

# Biomechanical Sensing and Algorithms

Joseph J. Lacirignola, James R. Williamson, Shakti K. Davis, and Whitney T. Young

Lincoln Laboratory has been developing software and hardware systems that can help determine if a soldier's performance has degraded due to fatigue, injury, or another detrimental physical state. Biomechanical data collected outdoors with commercial sensing devices have shown that several algorithms and models could interpret body movements to deduce a soldier's gait asymmetries, fatigue level, and amount of load carriage. Custom shoe inserts have been developed to measure lower-leg forces and movements in outdoor environments. The ability to acquire and interpret lower-leg measurements outside of a laboratory without compromising the natural rhythms of a person's gait facilitates the monitoring of complex biomechanical actions in military environments. Collecting lower-leg measurements outdoors can help researchers develop new models and methods for monitoring gait changes and improving military training to reduce the rate of musculoskeletal injuries.



**Lower-limb musculoskeletal injuries** (MSIs) are pervasive in military populations, with hundreds of thousands of MSIs reported every year [1]. These injuries include acute traumas (e.g., anterior cruciate ligament tears) and overuse injuries (e.g., stress fractures and medial tibial stress syndrome) [2, 3]. MSIs are a result of external stimuli and stressors, such as carrying a heavy load, that put strain on the complex biomechanical network of the lower legs. This network involves the interactions between muscles, joints, and the nervous system, and the dynamic forces and motions that result from such interactions. Training causes increased amounts of stress to load-bearing bones and joints because heavy load carriage and aggressive movements exert higher-than-normal forces on leg joints (hip, knee, and ankle) and bones (femur, fibula, tibia, and foot bones). Accurate measurements of the lower-leg forces and motions could inform decisions about how load is applied to each soldier during training and combat. These measurements could help prevent training injuries and lead to the development of training procedures that focus on maintaining a soldier's mobility and agility. Determining the dynamic forces and motions of the lower-limb movements and their interactions requires measuring lower-leg forces, acceleration, and displacements and using algorithms to elucidate the association between the different factors of lower-leg movement.

A variety of biomechanical sensors can be used to monitor leg movement, as shown in Figure 1. Measuring lower-leg forces and motions in a robust, repeatable

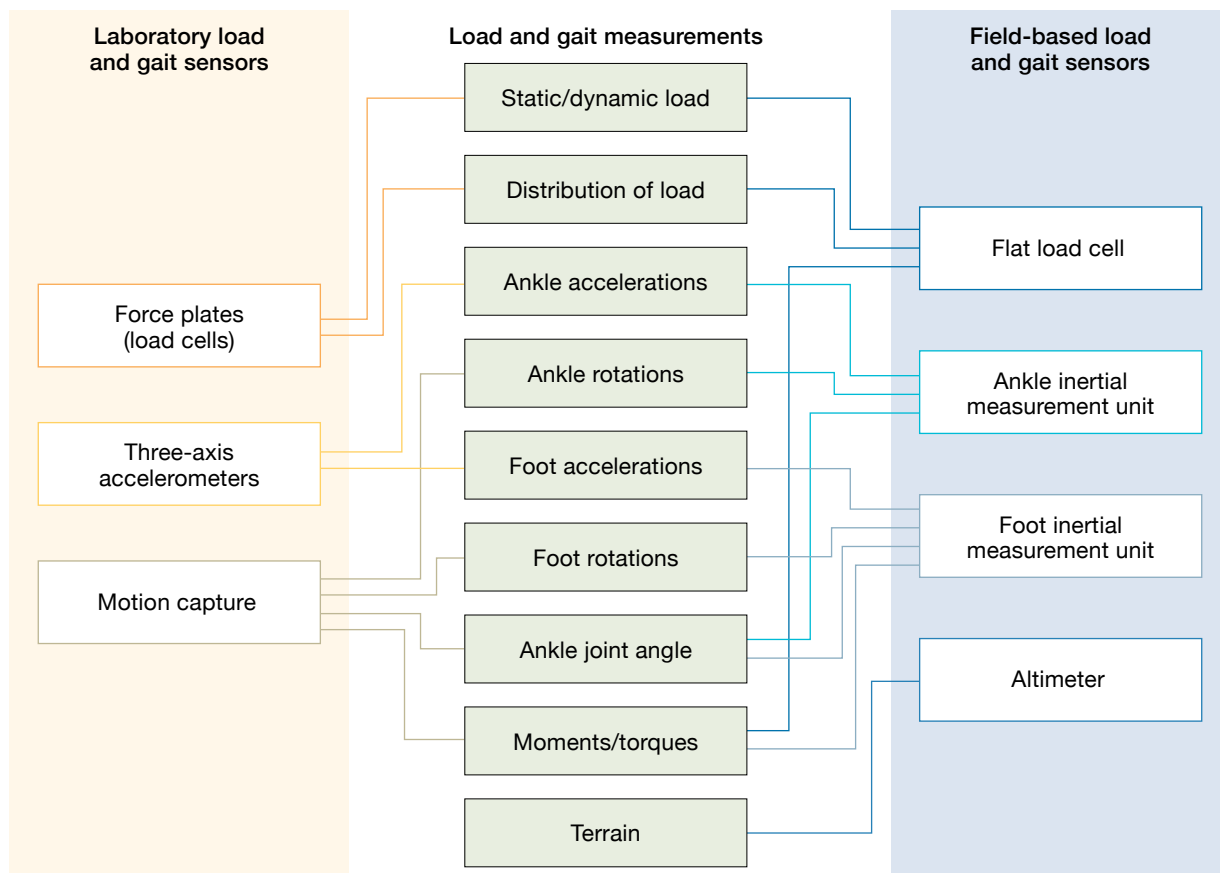


**FIGURE 1.** A comparison of laboratory- and field-based biomechanical measurement systems is illustrated. The far left column is a list of gold-standard laboratory load and gait sensors while the far right column is a list of field-based load and gait sensors. The middle column is a list of load and gait measurements. Lines from the laboratory and field sensors indicate which measurements can be optioned from each class of sensor.

manner is challenging to achieve outside the laboratory because existing biomechanical sensors are limited by factors such as a lack of accuracy or a design that impedes natural movement. Lower-leg kinematic gait models exist, but interpreting lower-leg measurements and turning them into actionable information is difficult because mobility, agility, or injury models do not exist.

In a laboratory setting, measuring lower-leg biomechanics is well established. Force plates and force-sensing treadmills measure ground reaction forces (GRFs), or the forces exerted by the ground on a body in contact with it. Fixed, multicamera motion-capture systems and accelerometers can directly quantify the kinematic and kinetic responses of lower-limb movement for static and dynamic conditions [4]. Although these laboratory-grade sensors are accurate and are considered the gold standard for biomechanical measurements,

they are cumbersome and difficult to translate to a field environment; thus, there is a lack of field data and a limited ability to determine the real-time impact of environmental stressors, such as different terrain types and sudden changes in elevation, on an individual’s mobility, agility, or susceptibility to injury. There is also a lack of persistent, long-duration measurements that explicate what role repetitive motion or fatigue plays in injury or reduction in agility and mobility. In addition, little is known about how lower-limb movements, forces, and accelerations change during unloaded or loaded activity prior to and after an MSI is incurred.

Advances in electronics miniaturization have enabled some conventional laboratory measurement methods, such as motion tracking, motion capture, and load or pressure sensing, to be incorporated into wearable devices. Taking these biomechanical measurements

outside of the laboratory is a big step toward gathering much-needed real-world data. However, several of the developed devices still fall short compared to their gold-standard laboratory counterparts. Commercial wrist, head, limb, or torso-based motion-tracking devices (e.g., Fitbit and heart rate monitors) have unobtrusive forms but lack the sampling rates and accuracy needed for comprehensive biomechanical analysis. Wearable motion-capture systems provide more accurate measurements than motion-tracking devices and are often accompanied by biomechanical models to relate the sensors to each other during movement. But the improvement in accuracy comes at the price of obtrusive design components (e.g., multiple long wires or battery packs), insufficient battery life (one to two hours), and susceptibility to magnetic interference.

Force-sensing shoes and shoe inserts can measure GRFs outside the laboratory. Sensors developed for these devices currently lack robustness, dynamic range, accuracy, and forms that do not alter gait. Additionally, this group of sensors does not yet have analytic packages that can detect gait anomalies or state changes in lower-leg movement.

Several commercially available accelerometers or inertial measurement units (IMUs) are small and wearable, and can support field-based measurements. Shoe- and chest-worn accelerometers can be used to determine basic gait features and estimate the weight carried by an individual. However, further research and development are needed to mature the state of models and algorithms for these types of sensors and to convert the raw IMU data into actionable biomechanical information.

### **Estimating Gait Asymmetry from Commercial Shoe-Mounted Accelerometers**

Gait asymmetry (nonidentical spatiotemporal parameters between limbs) can be a useful indicator of medical and pathological conditions, including MSIs, neurological damage associated with stroke or head trauma, and a variety of age-related disorders [11]. The ability of body-worn accelerometers to monitor and estimate gait asymmetry in real time can help researchers be aware of any medical conditions in a subject and administer timely interventions. At Lincoln Laboratory, accelerometers mounted on shoes have been used to measure an individual's foot motion during walking to estimate the

level of gait asymmetry. These estimates were achieved by computing simultaneous acceleration differences between the two feet to test the system's ability to reliably detect small asymmetries in the presence of natural variability in walking speeds and conditions. To test a gait asymmetry estimation algorithm, we conducted an experiment in which ankle weights were used to create asymmetries in the natural walking gait. The algorithm was able to estimate the direction and magnitude of gait asymmetries during continuous gait monitoring.

### **Gait Asymmetry Features**

Several types of gait features have been investigated to assess gait asymmetry: stride timing (swing or stance times) [5–8], acceleration magnitude [9], and acceleration time-varying patterns and the degree of similarity between given peaks (autocorrelation) [9, 10]. These features have primarily been assessed in the context of clinical or laboratory measurements compared against normative values. While many studies assume gait symmetry for normative values, even a healthy individual may not have a symmetric gait [11]. Establishing the baseline gait measurements of a healthy individual and obtaining individualized gait characteristics are useful in evaluating changes in gait over time. Individualized gait asymmetry detection is also important because there is natural variability between different subjects' gaits.

The Lincoln Laboratory gait asymmetry estimation algorithm uses novel statistical features that characterize asymmetry in acceleration magnitudes and dynamical patterns. These features are combined in an individualized algorithm that estimates gait asymmetry relative to the user's baseline gait measurements in variable contexts, such as different walking surfaces and speeds.

Statistical foot-motion features are computed from the acceleration magnitudes of the left and right feet within fixed 20-second time frames. These features, which do not rely on the detection of stride events, use simple computations that are easy to implement locally on the foot sensor. Two types of motion features, magnitude and pattern features, are computed at the sensors and then combined across the two feet to yield asymmetry features. Magnitude asymmetry is computed using the standard deviations of the left and right feet's

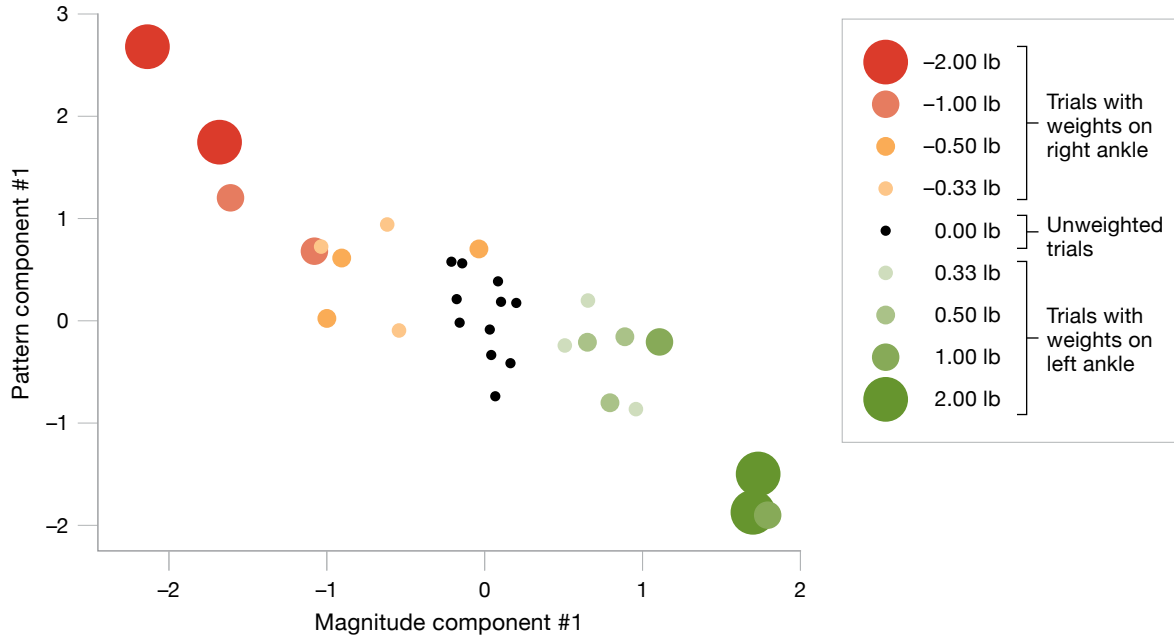


**FIGURE 2.** The mean feature values from 31 trials for Subject 6 are plotted above. On the x-axis is the magnitude feature, and on the y-axis is the first frame-based pattern principal component. Black circles indicate unweighted trials, shades of red indicate trials with weight on the right ankle, and shades of green indicate trials with weight on the left ankle. Marker size and shade indicate the size of ankle weights, which ranged from 0.33 to two pounds. The greater the induced weight of a trial (larger circles), the more the magnitude and pattern features deviate from those of the unweighted trials (small, black circles), indicating that gait asymmetry can be estimated from comparing the observed features.

magnitudes. Let  $x$  and  $y$  represent the standard deviation of the left and right feet’s acceleration magnitude signals, computed over the fixed time frame. The magnitude asymmetry is computed by using Equation (1), the symmetry index function [12].

$$SI(x, y) = \frac{x - y}{0.5(x + y)} \quad (1)$$

Pattern features register differences in the temporal stride dynamics between the two feet after magnitude differences have been factored out. Within-foot stride dynamics are captured by using autocorrelations of the acceleration magnitude signals. Autocorrelation peaks have been used by researchers to characterize gait from a single accelerometer [13]. In the Lincoln Laboratory algorithm, the autocorrelation function is regularly sampled out to the first peak, thereby representing time-delay correlation coefficients spanning a single stride. Differences between the autocorrelations of the two feet over these time delays constitute a raw pattern asymmetry feature vector. The first four principal components of this vector produce the final pattern asymmetry features.

### Estimating and Detecting Asymmetry

The gait pattern for a healthy, uninjured individual was characterized on the basis of a normal distribution obtained from training set features from the same individual with no induced asymmetry. The induced gait asymmetry was then detected by measuring the distance of gait features from the normal gait feature distribution. To induce gait asymmetries in a controlled manner for 24 subjects, we added a range of weights to each subject’s right or left ankle and obtained walking trial measurements. Figure 2 shows a scatter plot of the mean feature values computed from 31 separate indoor and outdoor walking trials for one subject. The scatter plot represents the magnitude asymmetry feature (symmetry index of standard deviation of acceleration magnitude) and the first pattern asymmetry feature (first principal component extracted from the autocorrelation differences). The unweighted trials are plotted with black circles. Right ankle-weighted trials are plotted with red circles and left ankle-weighted trials with green circles. The size of the circle indicates the magnitude of the weight. The magnitude and pattern features depend on which foot the load is applied to and the level of induced gait asymmetry.

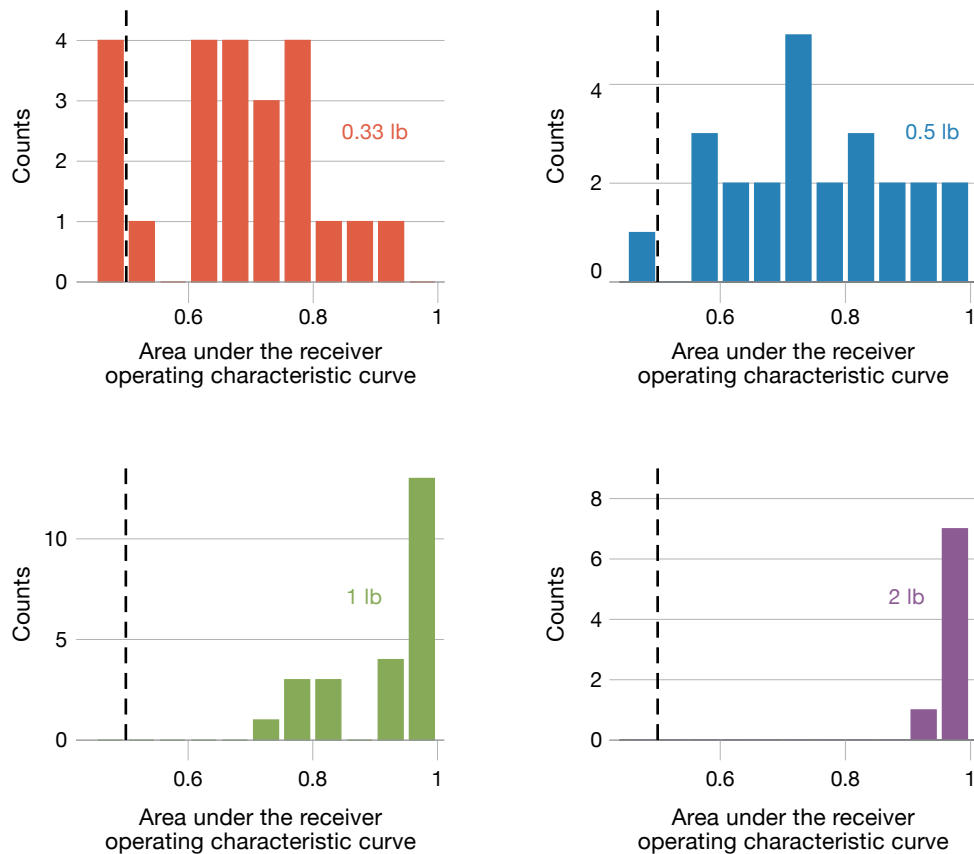


**FIGURE 3.** This figure shows histograms of gait asymmetry detection results across subjects in the four weighted conditions. Under each weight condition, an AUC (area under the receiver operating characteristic curve) value for each subject was computed that quantified the ability to detect the presence of an induced asymmetry in a trial when it is compared to unweighted control trials for the same subject. These histograms show the counts, across all the subjects, of different ranges of AUC values computed. AUC = 0.5 indicates chance-level accuracy and AUC = 1.0 indicates perfect accuracy. The trials with larger induced gait asymmetry had AUC distributions that were closer to 1.0, which means that these trials had a higher accuracy rate of asymmetry detection.

The trend for a single subject shown in Figure 2 holds across many subjects. Figure 3 summarizes the ability to detect, based on combined magnitude and pattern features, asymmetrical walking trials by using outlier detection. The outlier detection was performed by using subject-dependent background models constructed from three randomly selected unweighted walking trials. The distributions of an accuracy statistic, the area under the receiver operating characteristic curve (AUC), are plotted for four induced weight conditions. Larger induced gait asymmetries led to easier outlier detection.

### Case Study: Use of Commercial Sensors to Track Recovery from Injury

The results on induced asymmetries raised the question, “How does the algorithm perform on gait

asymmetries that arise from an actual overuse injury?” We addressed this question provisionally by analyzing data from a subject who developed iliotibial band syndrome, a common overuse injury [14], several weeks after the original study. To track this subject’s recovery, we recorded one trial of indoor walking over six days following injury diagnosis (Friday, then Monday through Friday of the following week). In Figure 4, the magnitude feature and raw pattern feature vectors are plotted over four days during the original collection (without induced asymmetries) and over six days during injury recovery. The subject reported the most discomfort and exhibited limping in the first two collections (Friday and Monday). The gait asymmetry features are consistent with the subject’s self-reported discomfort.

Prior to the injury, the magnitude feature from unweighted bouts in Figure 4 shows considerable stability over many days. After the injury, however, the magnitude feature becomes negative, indicating a left foot asymmetry. During the course of recovery (around six to seven days following the injury), the magnitude feature returns to its

pre-injury baseline. The multidimensional pattern features show a similar result. Immediately after the injury (days +1 and +4), the pattern feature vectors are clearly different from their pre-injury state. Notably, the pattern features show the greatest deviation from normalcy on day +4, when the subject reported the greatest level of discomfort

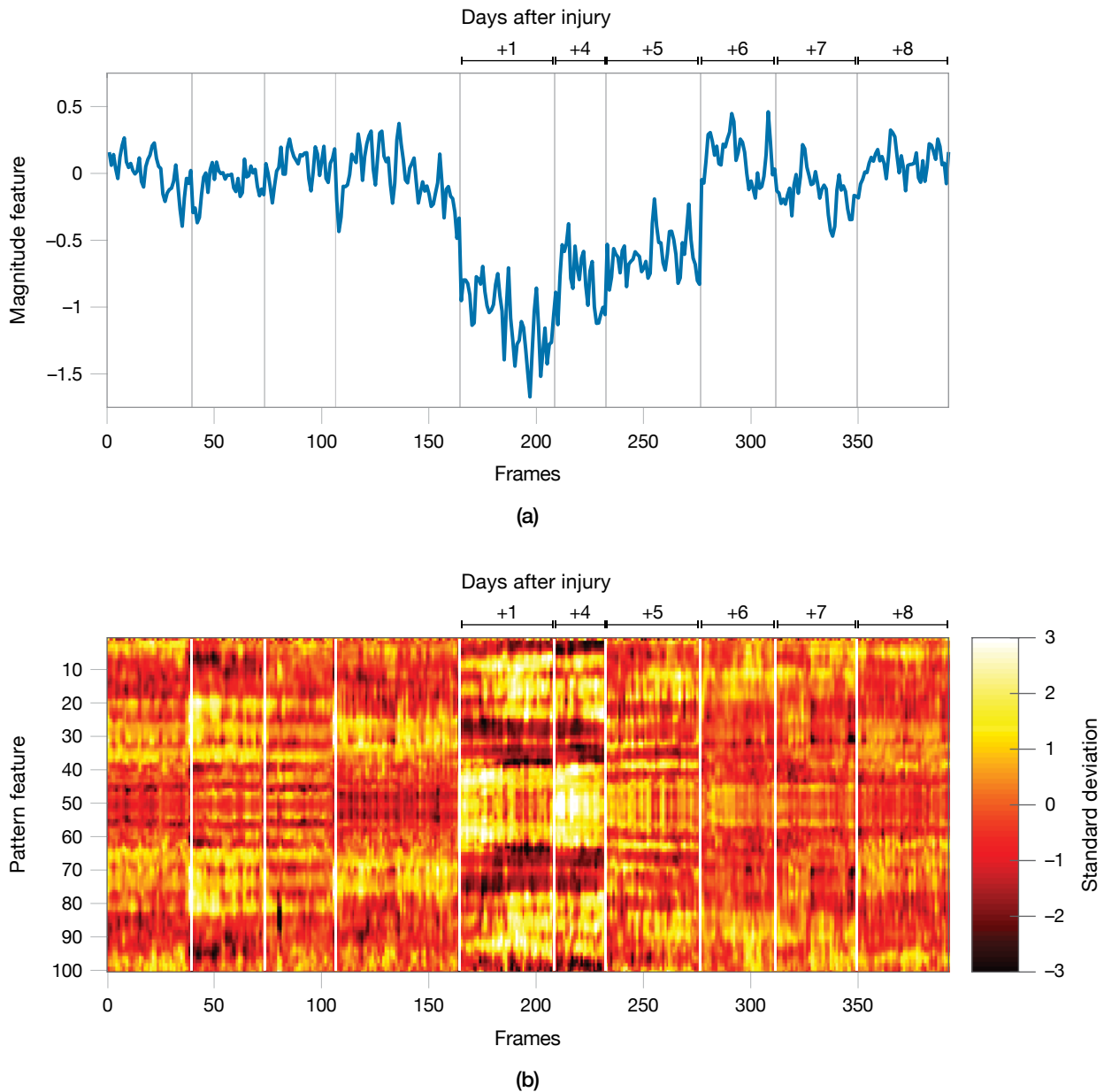


**FIGURE 4.** Frame-based magnitude feature values for a subject are shown before and after the repetitive stress injury (a). Magnitude features are plotted in units of standard deviation from the mean (following cross-frame normalization). Also plotted are the differences between the raw pattern feature vectors of the left and right feet (b). The detection algorithm uses principal component features, which are extracted from these high-dimensional vectors. The y-axis of Figure 2, for example, shows the first principal component of the pattern features. The changes in magnitude and pattern features correspond to the timing of the subject’s injury, indicating that the features tracked in this study have the potential to provide insight into real injuries.

and decided to stop walking halfway through the trial. This small-scale case study suggests that the feature set presented in this article has potential for detecting and tracking actual MSIs and subsequent recoveries.

### Estimating Load Carriage from a Commercial Torso-Mounted Accelerometer

Heavy loads increase the risk of MSIs for foot soldiers. Military personnel commonly engage in training and operational activities in which they carry heavy loads (77 to 143 pounds or more) that increase the risk of MSIs [15]. Real-time continuous monitoring of load carriage would improve the ability to assess these risks. In addition, characterizing the effect of load on gait dynamics could allow early detection of MSIs or thermal work strain by analyzing unusual gait patterns.

We used information from a body-worn accelerometer to develop a load-estimating algorithm. The algorithm extracts features that characterize movement dynamics from a commercial torso-mounted accelerometer and uses statistical models to map the features to load estimates. The algorithm obtains rapid estimates of load with robustness to changes in equipment configuration, walking conditions, and walking speeds. On a combined dataset of soldiers and civilians carrying loads that ranged

from 0 to 89 pounds, load estimates were obtained with correlation  $r = 0.91$  and mean absolute error <10 pounds.

The analysis focused on a five-kilometer march in which soldiers carried different loads corresponding to different equipment configurations. Each soldier wore different equipment on different days. The total march durations varied between 40 and 68 minutes. The soldier data were augmented by civilian data collected from trials at Lincoln Laboratory in which 31 volunteers (19 men and 12 women) between the ages of 18 and 65 wore the Equival EQ-02 heart-rate monitor/accelerometer during natural walking. For 26 of these subjects, we compiled a single trial of unloaded walking data from multiple indoor and outdoor walking segments. The outdoor walking took place on a looped 0.4-kilometer gravel path that included uneven terrain and an eight-meter elevation change. Five subjects walked only outdoors, with loads of 0, 20, and (for one subject) 41 pounds. A weighted backpack was the load.

Figure 5 shows the raw acceleration data from a single soldier bearing a moderate load of 45.2 pounds (a) and a heavy load of 84.2 pounds (b). The plots represent 10 seconds of a 60-second data frame that has been converted to standard units (z-scoring) with three time series vertically offset for easy viewing.

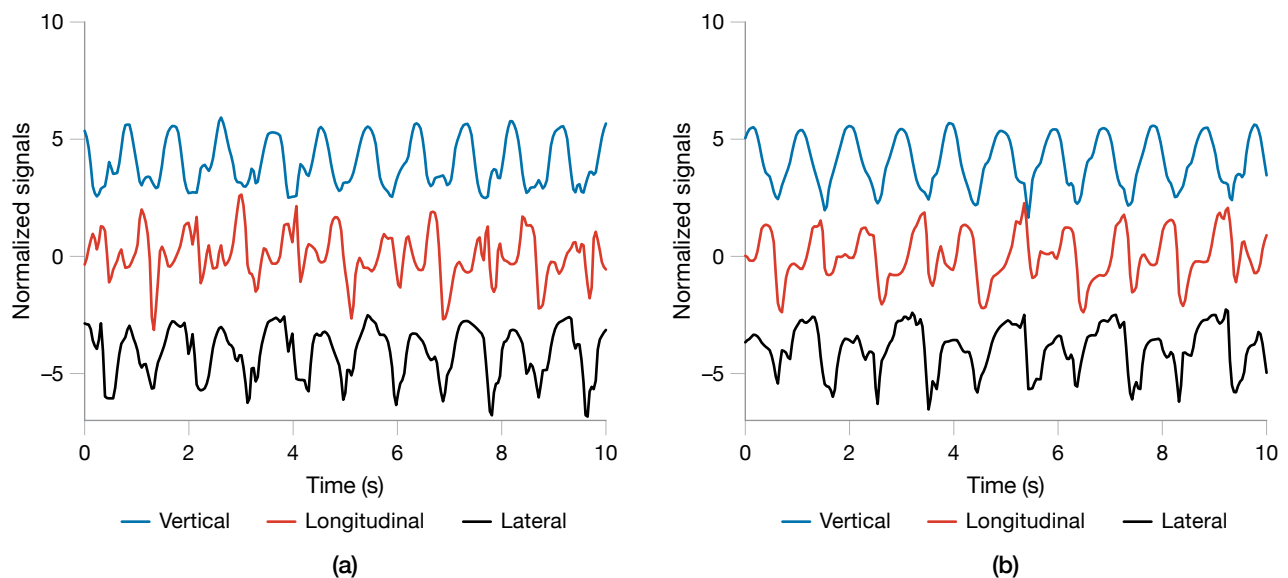


**FIGURE 5.** The graphs show acceleration signals from the same soldier carrying a load of 45.2 pounds (a) and 84.2 pounds (b). The signals are plotted in standard units (with 0 being the mean), z-scored within 60-second frames, and offset for easy viewing. Vertical, longitudinal, and lateral refer to the axes of measured acceleration relative to the torso. Autocorrelation shape features, shown in Figure 6, can be used to make inferences about the effect of load carriage on acceleration for each axis.

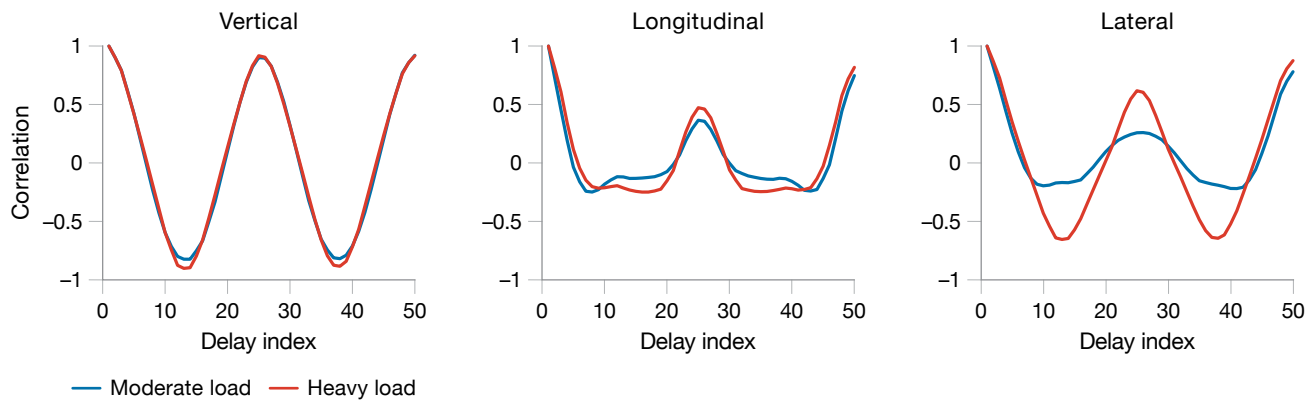


**FIGURE 6.** Depicted are the autocorrelation shape features, which are the time-scaled autocorrelation patterns for the three axes described in the data frames illustrated in Figure 5. The longitudinal and lateral axes show the largest changes between the moderate (blue) and heavy (red) loads. These results indicate that increasing load carriage causes the largest changes to the dynamics of acceleration in the longitudinal and lateral movement directions.

Autocorrelation shape features that are based on time-scaled autocorrelation patterns are used to analyze the dynamics within each accelerometer axis separately, (Figure 6). These autocorrelation patterns are plotted over a range of time delays that span the average duration of a single stride. The differences between the moderate load (blue) and heavy load (red) autocorrelation patterns, particularly in the longitudinal and lateral axes, indicate a basis for discriminating load levels.

We use correlation structure features to holistically characterize relationships across the three acceleration axes and across time delays. This analysis is done by constructing high-dimensional correlation matrices by employing time-delay embedding, such that each matrix represents a full set of correlations within and across acceleration axes at a set of relative time delays. We then use the matrix eigenspectra to quantify torso dynamics properties. Figure 7 shows that the correlation structure features (the matrix eigenspectra) obtained from a heavy load (red) differ from those obtained from a moderate load (blue) for the same subject. The reduction of lower-rank eigenvalues with load indicates a reduction in torso dynamics with fewer independent modes of motion.

The autocorrelation shape features and the correlation structure features were mapped into load predictions by using a regression algorithm, which is trained on held-out subjects by applying leave-one-subject-out cross-validation [16]. The load-estimation algorithm is applied to a combined dataset consisting of loads ranging between 0 and 89 pounds. The algorithm is able to predict loads

with high accuracy, producing estimates with a mean absolute error of 9.57 pounds and a Pearson correlation with true loads of  $r = 0.91$ . Figure 8 shows a scatter plot of estimated load as a function of true loads, with a linear regression fit to the estimates shown in red. Despite the high overall correlation between estimated and true load, some error in the load estimates remains. Further testing has indicated that much of this remaining error may be attributed to cross-subject differences in body morphology that result in different levels of change in torso dynamics given the same absolute load. Excessive trunk swaying from fatigue or an unbalanced load may also hinder the algorithm's ability to estimate load. A path for future research is to automatically calibrate the load algorithm for each individual, allowing the algorithm to more accurately track within-subject changes in load over time.

The techniques introduced in this section, which characterize complementary properties of accelerometer movement dynamics, could prove useful for other applications, such as early detection of MSIs, detection of excessive thermal work strain, and monitoring of physical fatigue. We extended this work to consider estimating biomechanical state characteristics from a wide variety of sensors.

### Multimodal Measurements for Biomechanical Analysis

Body-worn accelerometers can be used to detect gait acceleration differences and can give an estimate of load carried, but more information is needed to truly

understand and interpret more complex and long-duration dynamic movement, namely accelerations and rotations of the feet and ankles, GRFs, and characteristics of the local terrain. While wearable sensors exist for each of these three measurements, no commercial system combines the three modalities for lower-leg biomechanical measurements, and the analytical tools needed to comprehensively integrate the multimodal sensors and interpret lower-leg movement are still an area of open research.

Recently, sensors embedded within or near footwear [17] have increased the possibility for field GRF measurements [18]. Several of these technologies include modified insoles, such as pressure-sensitive fabrics [19], force-sensitive resistors [20], and capacitive arrays [21]. These approaches have excellent packages and are compatible with many types of footwear, but they are limited in dynamic range, sampling frequency, and accuracy. In-shoe technologies often use small load cells and force plates integrated around a sandal [22, 23] or underneath a soldier's boot [24]. While the in-shoe approaches tend to demonstrate higher accuracy and more robustness compared to insole measurements, they are expensive, and their large size and weight tend to alter the normal gait of the user. These commercial and research-based load measurement systems represent progress toward ambulatory sensing; however, they are not complete systems and lack the integration of all the sensing modalities needed for measuring lower-limb biomechanics. To truly understand lower-leg biomechanics, GRF and movement sensors need to be combined into a portable, nonobtrusive format.

Direct measurement of GRFs allows researchers to calculate the dynamic forces of the foot. These dynamic forces, in combination with foot and ankle motion measured by IMUs, may allow the calculation of dynamic forces around the ankle joint. GRF and terrain measurements could also play a role in estimating energy expenditure and inform strategies for load carriage configurations that minimize injuries and maximize performance over a variety of terrains.

To address the gap in multimodal sensors and field measurements, we developed a lower-leg biomechanical measurement system called the Mobility and Biomechanics Insert for Load Evaluation (MoBILE). The MoBILE system combines a shoe insert that captures foot measurements with an ankle sensor. The insert measures

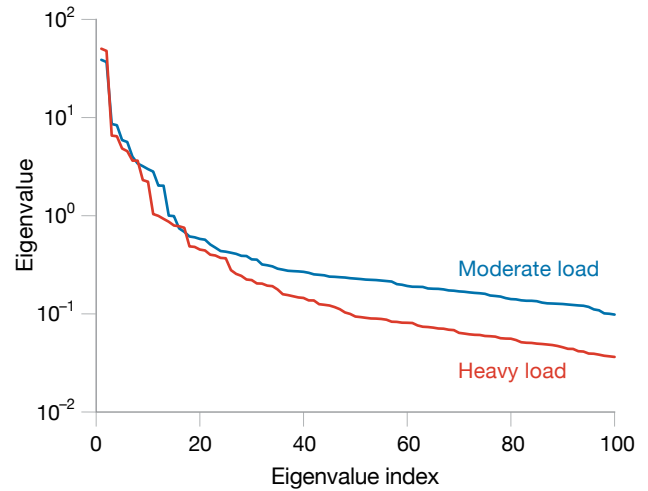


**FIGURE 7.** Depicted above are the channel-delay correlation matrix eigenvalues for a moderate load (blue) and for a heavy load (red). The heavy load causes a reduction in magnitude at the low-rank eigenvalues.

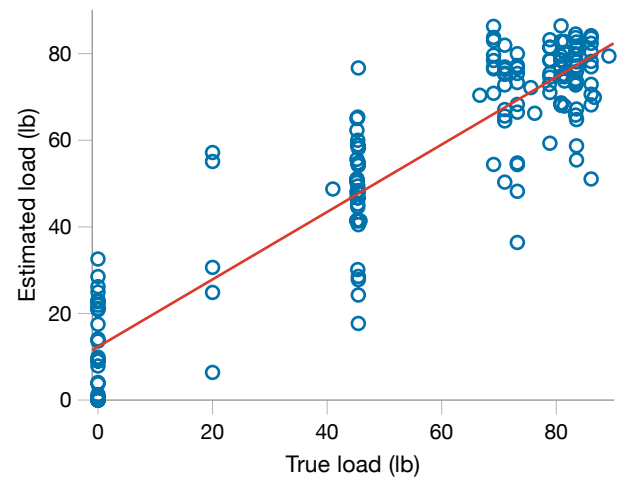


**FIGURE 8.** The plot shows the estimated load as a function of true load for the combined dataset consisting of 125 soldier trials ( $\geq 45$  pounds) and 37 Lincoln Laboratory trials ( $\leq 42$  pounds). The algorithm obtained predictions with a mean absolute error of  $< 10$  pounds and correlation  $> 0.9$ . The plot demonstrates a high overall correlation between estimated and true load, though some error remains because of factors such as variability between subjects' bodies.

GRFs at the toe, arch, and heel of each foot by using custom-designed, inexpensive, flat, and flexible load cells (Figure 9). These novel load-sensing elements have a large dynamic range (up to 3,530 Newtons or 800 pounds) and measure vertical GRFs at high sampling rates. In addition to having GRF sensors, MoBILE also incorporates

nine-axis IMUs (three axes each for the accelerometer, gyrometer, and magnetometer) at each foot and above each ankle and a barometer in the ankle sensor package to measure local terrain features (Figure 9).

The load-sensing elements in each insert, constructed with strain gauges, measure ground resistance in response to changes in load. To convert resistance to load, we used an Instron loading apparatus to determine static (standard curve) and dynamic (creep test) material property parameters for each sensor. The material properties can be used in a viscoelastic model to characterize the viscous and elastic material components to account for the influence of the rubber and foam insert material on the output resistance [25].

The compact MoBILE ankle package integrates the sensors with readout electronics, high-rate data storage, and a rechargeable battery to enable offline analysis of locomotion without altering the mobility of the wearer. We used the system to characterize stationary measurements of weight and dynamic responses (e.g., during walking and running) and directly compared the results to measurements of a force-sensing treadmill. We are also developing analysis tools to evaluate changes in biomechanical gait state during prolonged exercise or training events, and we are developing data-driven algorithms to interpret the large quantity of measured data. Our goal is to characterize an individual's biomechanical state and detect precursors of MSIs in the lower limbs before load-related injuries are incurred.

### MoBILE Dataset

The MoBILE system records a rich, high-dimensional set of data. A nominal recording includes data from two sets of load sensors (toe, arch, and heel sensors on each foot), four nine-axis IMUs (one on each foot and each ankle), and two barometric pressure sensors (one on each ankle). This configuration results in 44 independent and concurrent data streams available for analysis. Most of the MoBILE sensors are sampled at rates that are compatible with those of laboratory-grade sensors, with an overall data rate of more than 7,000 samples per second (Table 1). The MoBILE system yields high-resolution data that are recorded and stored for algorithm development, state classification, and anomaly detection.

The data analysis incorporates many well-established gait features from the literature, including cadence and

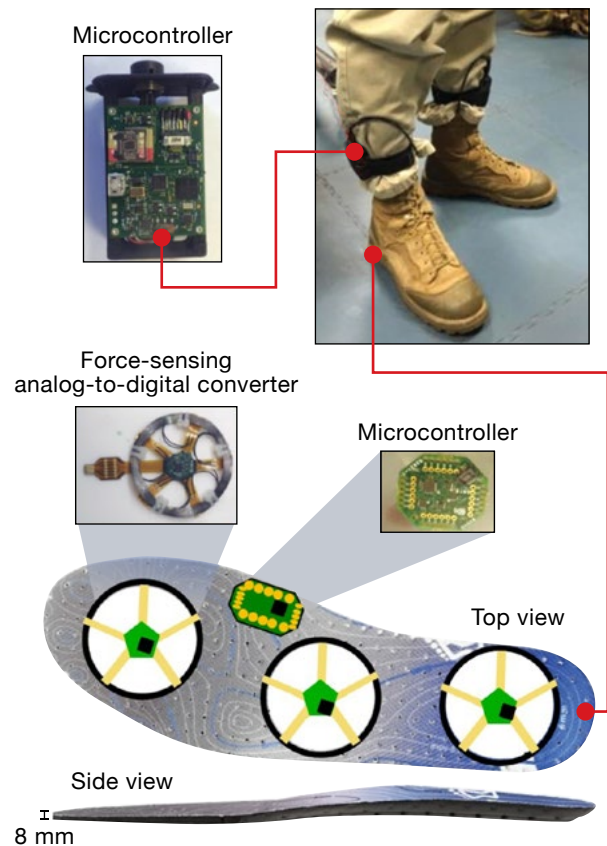


**FIGURE 9.** Lincoln Laboratory has developed the Mobility and Biomechanics Insert for Load Evaluation (MoBILE), which includes a nine-axis inertial measurement unit for each foot and ankle and a left and right shoe insert that measures ground reaction forces at the toe, arch, and heel of each foot. Each insert and ankle unit contains a microcontroller unit and an analog-to-digital converter and associated electronics.

foot-contact time. The addition of concurrent data from multiple sensors enables the investigation of many new features, such as the peak forces of the heel and toe, and the relative timing of events within the gait period. The rich datasets support the exploration of many more load-based features, ranging from timing and magnitude values within and across the sensors, to symmetry indices similar to those explored in accelerometry, to statistical and information-theoretic features like kurtosis and entropy that characterize the shape or content of the signal waveforms.

### Data Preprocessing

After downloading the raw set of measurements from MoBILE, we segmented the data into 10-second windows with five seconds of overlap. Within each window, two

main types of features are extracted: window based and stride based. Window-based features are summary statistics of the entire 10-second duration of a window, such as mean foot acceleration magnitude. These features characterize overall trends in the sensor values without explicitly segmenting the individual strides. To extract intra-stride events, such as the heel strike and toe off, it is necessary to determine which windows contain ambulatory motion. Windows with ambulatory motion are detected by setting threshold levels on the foot gyrometer energy and standard deviation. When the thresholds are exceeded, a window is classified as active, and the start of each individual stride is detected. Stride-based features are calculated for each individual stride in the 10-second window and reported as summary values (e.g., mean, standard deviation, median) within that window. An example of a stride-based feature is mean resistance at the heel strike. The sum of all three load-sensing elements is used to parse the load data into strides, and the foot acceleration magnitude is used to parse the IMU data. Both stride-parsing algorithms use a template-matching scheme to identify individual steps. When truth data, such as the start time, rest periods, trips, and falls, are available, truth annotations are overlaid on the data to support analysis and the development of supervised classifiers to predict anomalous gait patterns.

When biomechanical data are measured over a short baseline period (a few minutes), a normal gait characterization, including nominal gait and weight distribution features, can be established for an individual. Deviations from the baseline may provide insight into the individual's physical status to inform injury avoidance, mission readiness assessment, or performance enhancement. With the goal of characterizing meaningful biomechanical changes over time, we are conducting research to understand

which features are important for predicting health and performance or for providing actionable feedback on an individual's physical state.

### Activity Maps

As a way to get an overview of the data, activity maps can be generated to visualize trends across the data streams throughout the gait cycle. One way to construct an activity map is to segment the data into distinct events, such as portions of a data collection. Once segmented, the data can be visually inspected for changes or for the emergence of trends when different conditions are compared (for example, walking with and without a heavy load). This comparison can provide guidance on which data streams and/or time points may be strong candidates for feature extraction in the subsequent analysis.

As an example, Figure 10 shows activity maps during a walk with summary data from different time points during the walk. The maps show accelerometer and gyrometer data from the left and right feet and left and right ankles. In this example, the acceleration and gyration standard deviations are changing during the course of the walk.

### Deriving Altitude Rate from Barometric Pressure

The barometric pressure sensor in the MoBILE system tracks relative changes in barometric pressure over time. Although in theory, barometric sensor measurements could be converted to absolute elevation changes, some challenges make the conversion impractical. In particular, understanding the relationship between barometric pressure and absolute elevation relies on knowing the local atmospheric pressure, which can change rapidly over time and space. Rather than aiming to estimate absolute elevation, a more practical approach is to estimate relative altitude changes over short intervals

**Table 1. Summary of MoBILE Sensors and Data**

SENSOR TYPE	AXES	NUMBER	TOTAL	SAMPLING RATE
Load	3	2	6	Up to 600 Hz
Inertial measurement unit	9	4	36	100 Hz
Altimeter	1	2	2	15 Hz

of time during which the local atmospheric pressure is assumed to be constant. Calculating a moving average of relative altitude change or altitude rate provides important context about the terrain.

Figure 11 illustrates the derived altitude rate from the MoBILE system for a round-trip march over a hilly path and compares it to a reference elevation profile extracted from Google Earth for the same hilly path. Notably, the altitude rate calculation gives reliable estimates of when the subject is walking on flat terrain versus walking up or down moderate or steep hills. This information provides valuable context for interpreting lower-leg motion features.

**MoBILE Inertial Measurement Unit Data**

As previously described, we can detect gait asymmetry from foot-mounted accelerometers [26]. The inclusion of nine-axis IMUs in the MoBILE system allows for the expansion of gait analysis to include foot gyration and ankle acceleration, gyration, and magnetometer data. The concurrent measurement of 36 axes of motion in the MoBILE system leads to the extraction of hundreds of IMU-based features.

Window-based features such as the mean, median, and standard deviation of each axis (and associated magnitudes) can provide insight into general trends for each sensor over time or in response to relatively slow-changing conditions. Stride-based features allow for tracking more precise changes, such as the value of each sensor at stride landmarks (e.g., heel strike or toe off). Parsing the data into strides also supports the calculation of commonly used timing features, such as foot-to-ground contact time, cadence, percentage of time in stance, and percentage of time in swing. Figure 12 shows an example data window and the average stride across the window for each axis of the foot accelerometer.

After extracting IMU window- and stride-based features, we can perform additional analyses and comparisons. Symmetry, or lack thereof, between right and left gait features is a powerful indicator of gait anomalies (e.g., tripping) or gait asymmetries. The emergence of a gait asymmetry over time may be indicative of changes in stability, mobility, agility, or injury state. To further explore the indications of gait symmetry, we calculated symmetry indices as defined by Equation (1) for each IMU feature.

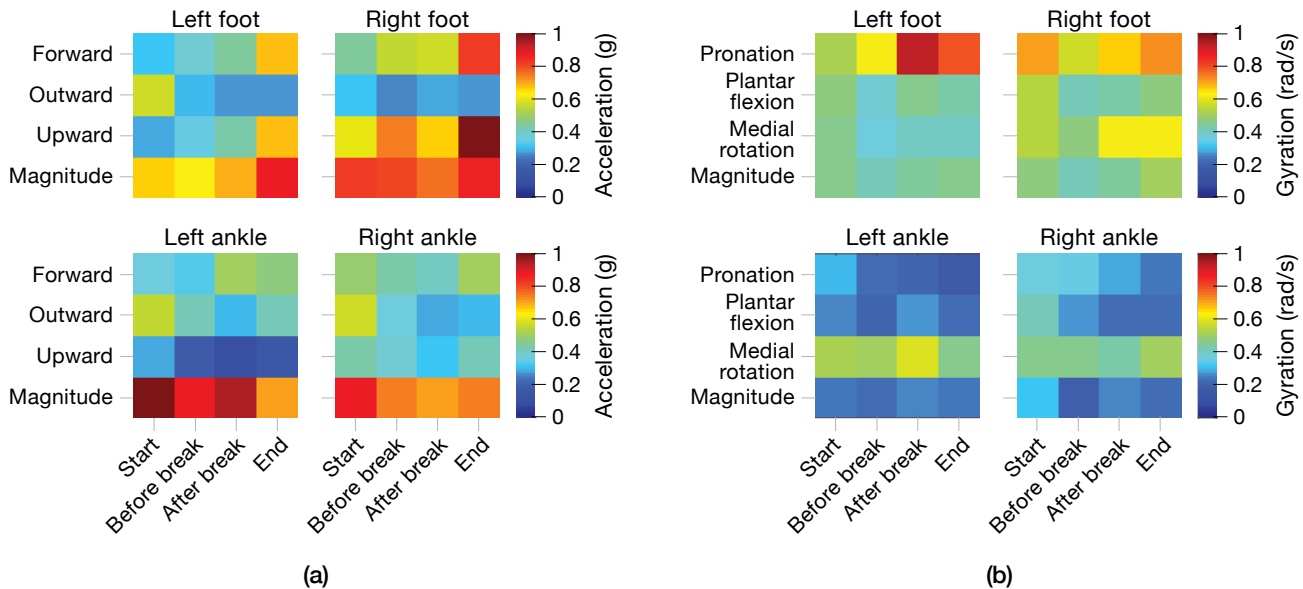


**FIGURE 10.** Example foot IMU sensor activity maps are depicted. The plots in (a) show the acceleration axis at different points during a march. The plots in (b) show the gyration axis at different times during a march. Pronation, plantar flexion, and medial rotation refer to different states in which the foot is flexed or rotated. The acceleration patterns show a difference in magnitude between the two feet throughout the data collection. The gyration pattern indicates a sharp change in the left foot pronation (collapsing of the foot arch upon contact with the ground) during the second portion of the walk.

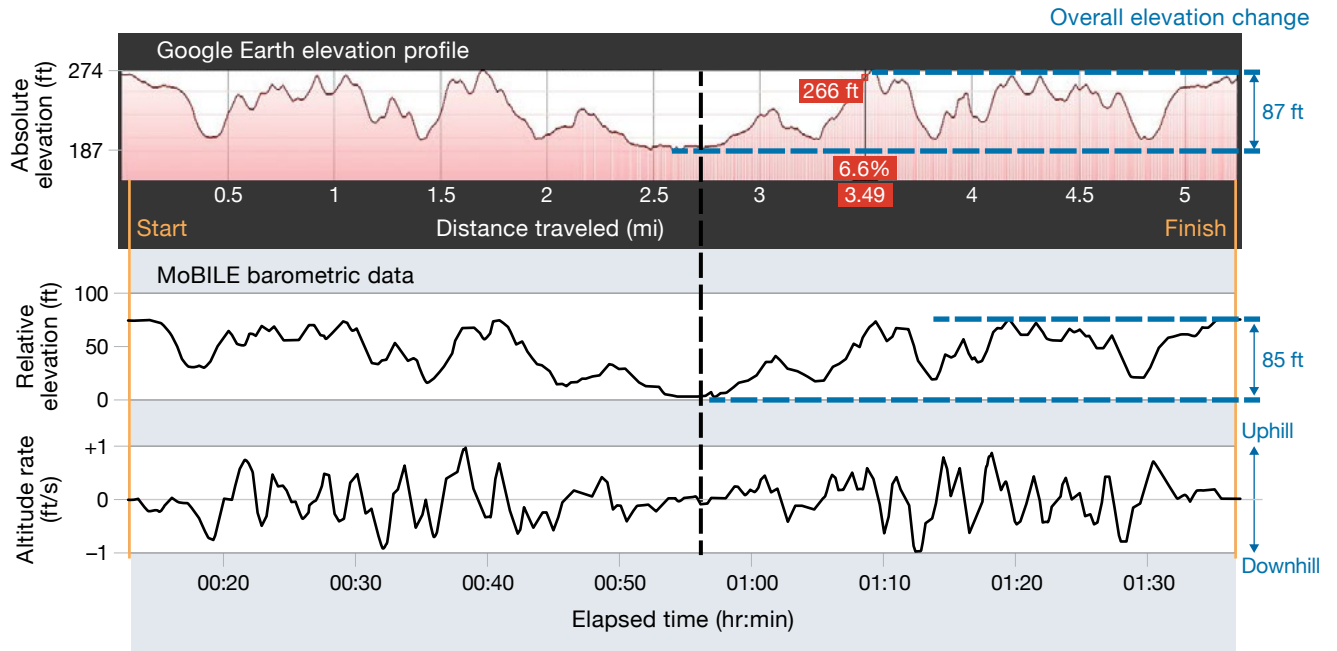


**FIGURE 11.** The figure shows the comparison of the MoBILE pressure sensor and altitude rate calculations with the Google Earth elevation profile. The MoBILE barometric data match the Google Earth elevation profile, indicating that the MoBILE sensor can provide a reliable picture of the terrain traversed by the user.

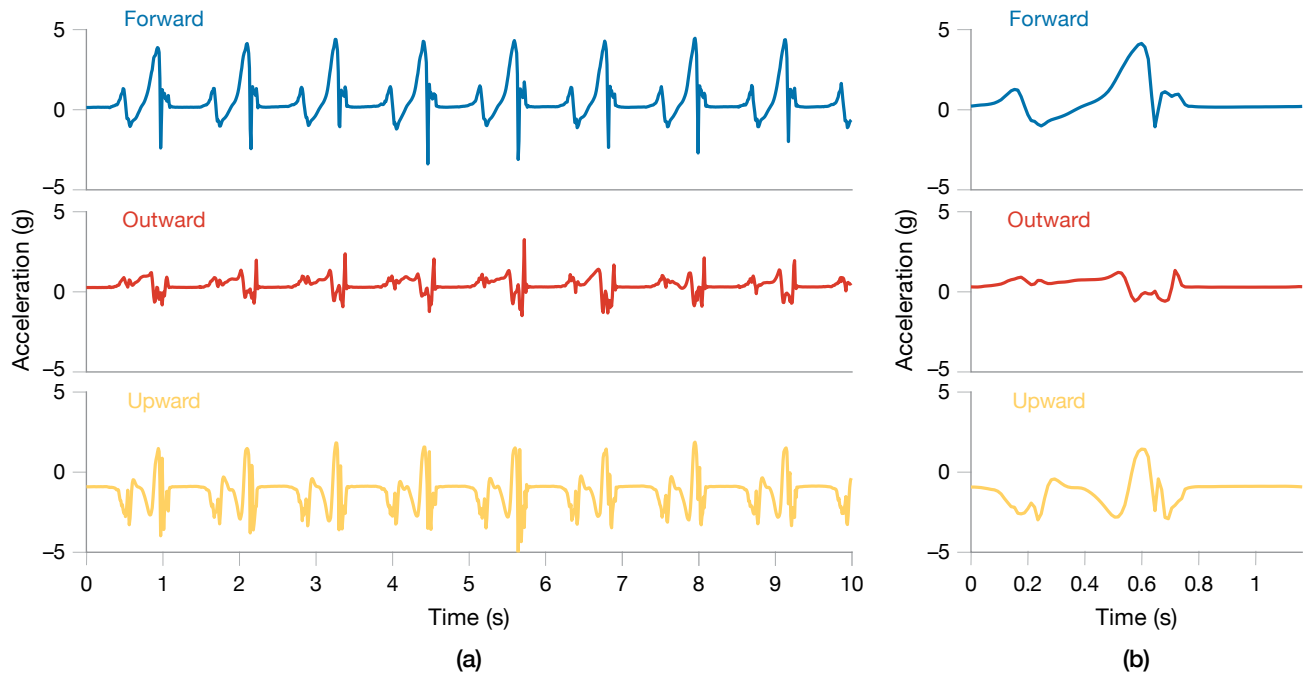


**FIGURE 12.** The graphs show an example of raw foot-accelerometer data gathered from the three axes of the accelerometer. The traces in (a) represent typical data seen in a 10-second window, and the traces in (b) show the accelerations for one average stride.

The IMU features can also be plotted in relation to condition changes, such as the change in altitude over time (altitude rate). Comparing features to altitude rate highlights terrain dependencies. Identifying such correlations can help deconvolve confounding factors, such as changes in gait due to terrain features, in later analysis involving classifiers. In Figure 13, the foot contact time (FCT) and plantar flexion gyration, both stride-based features derived from the foot IMUs, are plotted as a function of altitude rate. Each point on the plot represents a 10-second window during a 10-kilometer march across hilly terrain. The mean FCT has a strong increasing trend versus altitude rate, while the plantar flexion shows a strong decreasing trend versus altitude rate.

Comparing the time evolution of IMU features' baseline values for an individual has the potential to reveal patterns in the data that correlate with biomechanical state changes associated with conditions such as heavy load, fatigue, and varying terrain. Figure 14 shows four example foot IMU features versus load. To avoid the confounding impact of terrain change, the feature comparisons are restricted to windows in which the altitude rate is very small, consistent with the flat region in Figure 13. The symmetry indices show little to no change between a baseline walk (collected the day before the march with no external load) and the initial segment of a 10-kilometer march with a 40-pound load. The symmetry indices do change, however, after the subject walks for an extended period (approximately one hour) with a load. Other features show a significant change from a baseline walk to a walk with load while also showing further change after prolonged walking with a load. All of these features may indicate physical fatigue.

Future IMU work will include additional feature extraction, identification of the best candidate features, collection of more and larger datasets, development of classification algorithms, and multisensor data fusion. In addition, we will incorporate the ankle IMU data and the three magnetometer axes from each IMU into the analysis. Adding the ankle IMU data will allow for the calculation of ankle-specific metrics, inference into the status of the ankle joint, and correlations between the foot and ankle IMU measurements.

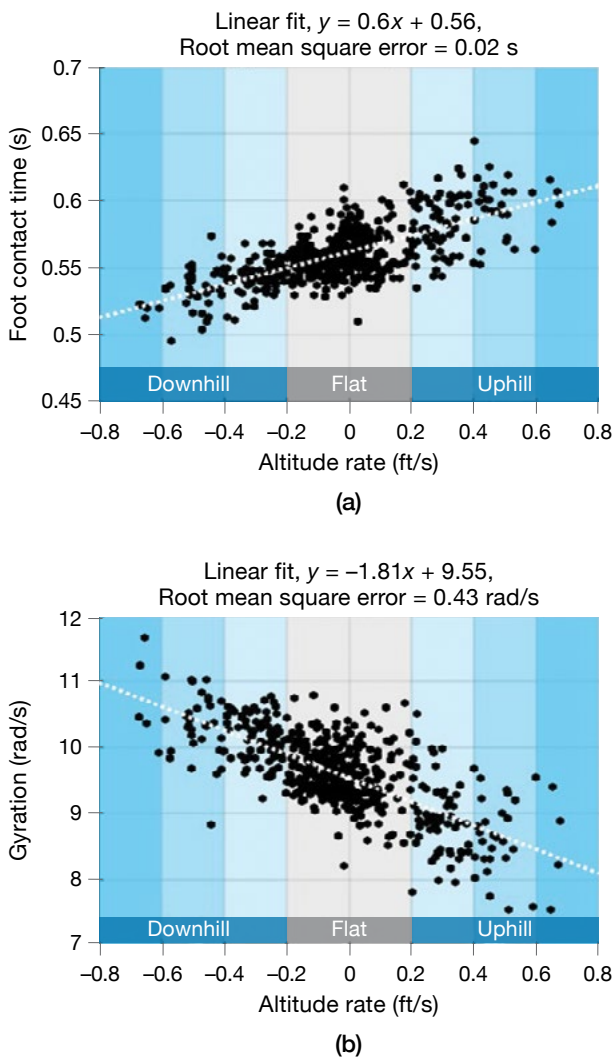


**FIGURE 13.** The plots show IMU features versus altitude rate and the associated root mean square error (RMSE). The foot contact time (FCT) and gyration vary depending on the terrain feature. For example, the FCT increases and gyration decreases during an uphill walk. The FCT decreases and the gyration increases during a downhill walk. These results indicate that the user is moving slower and has less foot rotation while walking uphill and is moving faster with greater foot rotation while walking downhill.

**Load Sensor Data**

The raw data from the load-sensing elements, prior to calibration, measure the strain gauge resistance in ohms. The load sensors at the heel, arch, and toe in the MoBILE insert capture the dynamics of the weight distribution across each foot. Figure 15 shows an example of the resistance measured at each sensor during several steps. Six

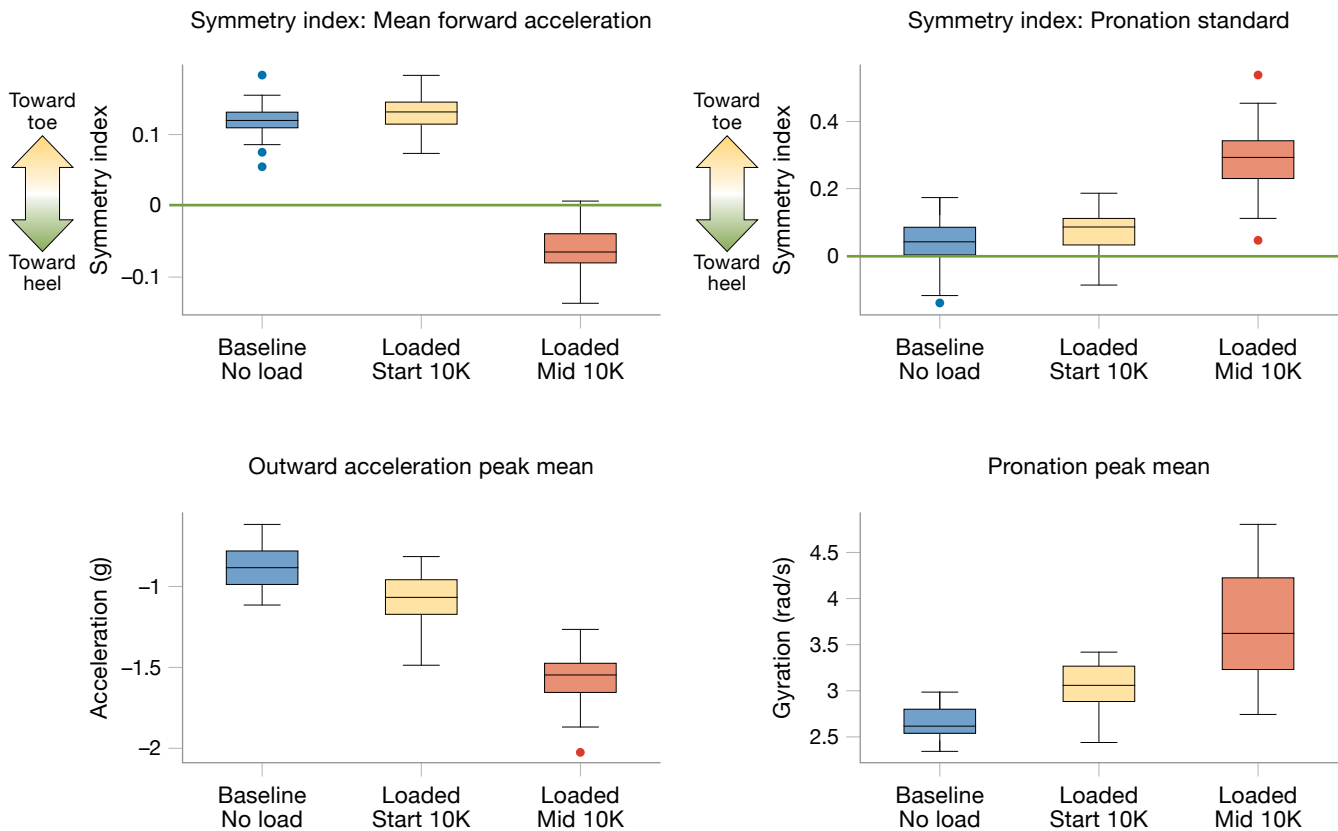


**FIGURE 14.** Depicted are foot IMU features versus load for a 50-step walking segment ( $N = 50$ ). The symmetry indices for mean forward acceleration and pronation standard deviation show little to no change during the no-load baseline and the start of a walk with a heavy load. There is a shift in both features after the subject has walked for approximately one hour. Other features, such as outward acceleration and peak mean pronation, show a steady change between no-load baselines, the start of the loaded walk, and after walking with a load for an hour.

consecutive gait cycles from a 10-second frame of data have been overlaid, showing only minor variations of weight distribution from one stride to the next within a frame. The heel, shown in red, is the first point of contact in the step and forms a sharp peak, referred to as the heel strike. Approaching mid-stance, the weight shifts from the heel to a balance between the toe and heel. Although the arch sensor is active throughout most of the stride, it bears only a small portion of the weight compared to the toe and heel. At the end of the stride, the toe sensor forms a peak as the foot begins to unload in an event known as the toe off. Conventional force plates measure a load profile similar to the black lines, which represent the sum of all three sensors.

We can infer many important gait characteristics, including the stride timing and the peak force associated

with the heel strike and toe off, from the overall weight profile. The addition of sensors in different regions of the shoe insert also provides a unique opportunity to detect anomalies in weight carriage in the heel, arch, or toe as physical and physiological conditions change. We estimated the resulting force from each sensor by using a viscoelastic model and the time-dependent deformation (creep) properties found during calibration of the insert [30].

Similar to features of the IMU, features derived from the load sensor insert were strongly correlated with changes in altitude rate (uphill, downhill, flat). Figure 16 shows the peak heel and toe force (after calibration) from a 10-kilometer road march in which a 188-pound subject wore a 40-pound vest. The heel strike data show a strong decreasing trend versus altitude rate. The toe sensor is

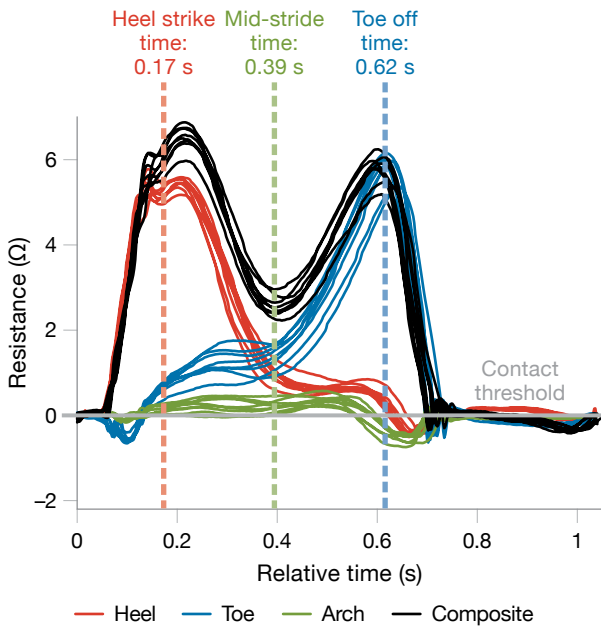


**FIGURE 15.** The figure shows the MoBILE load sensor resistance measurements from one foot. Data from six gait cycles in a 10-second frame are shown. At the beginning of the stride, resistance peaks at the heel, then shifts to a balance between the heel and the toe, and finally forms a peak at the toe at the end of the stride. The arch bears the smallest portion of the weight. The lines represent the sum of all three sensors.

less sensitive to terrain, and its data show only a slight increasing trend with altitude rate. Tracking weight distribution on the foot as elevation changes may be a good indicator of load carriage configuration or fatigue. In addition, any analysis will need to understand and account for weight distribution as it relates to altitude rate to separate terrain-related changes from changes that result from fatigue or injury.

Each insert measures load at three points under the foot. Using data collected by these inserts, we can estimate and monitor a center of pressure calculation throughout a collection. The center of pressure is a function of the load at different points on the foot in relation to a reference line (center of insert) as illustrated in Figure 17.

Center of pressure (CoP) is calculated at time  $t$  as

$$CoP(t) = \frac{d_{toe} f_{toe}(t) + d_{arch} f_{arch}(t) + d_{heel} f_{heel}(t)}{f_{toe}(t) + f_{arch}(t) + f_{heel}(t)}$$

where  $d_x$  is the distance from the center line of the insert

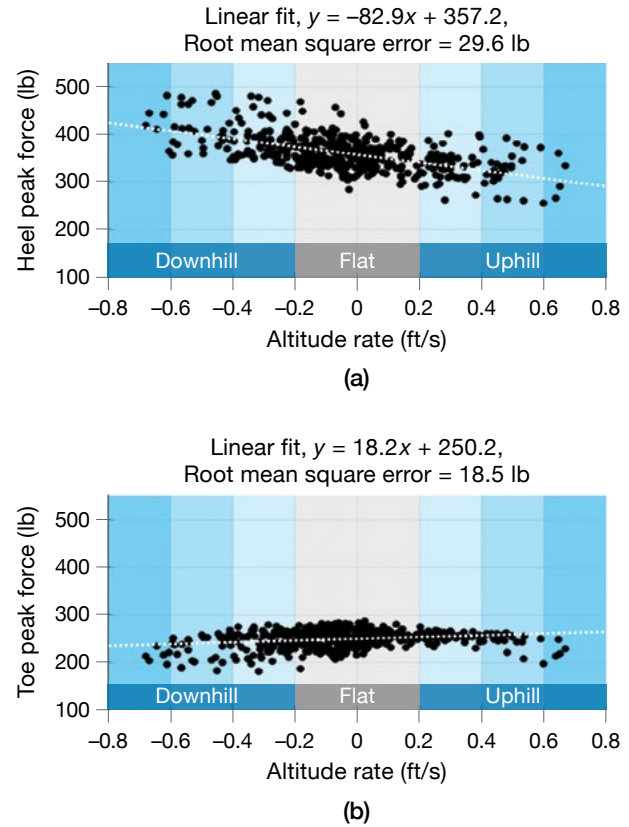


**FIGURE 16.** The plots show load distribution as a function of elevation. The heel (a) and toe (b) force data from the load sensor insert were strongly correlated with changes in altitude rate. These results indicate that the subject's weight shifted while walking uphill, downhill, or on flat terrain. The measurements of weight distribution on the feet as the terrain changes may be a good indication of the type of load carriage configuration or fatigue. Models will need to interpret and account for weight distribution as it relates to altitude rate to distinguish changes in weight distribution due to terrain from changes due to fatigue.

to the center of sensor  $x$ , and  $f_x(t)$  is the force measured at sensor  $x$  at time  $t$ . The variable  $x$  here indicates the toe, arch, or heel sensor.

Following the stride-based feature approach used in the IMU, we parsed the load data into individual strides and estimated the center of pressure for each stride on the basis of the heel-strike force versus the mid-stride arch force and the toe-off force. Examples of the center of pressure mean and standard deviation for each stride window are shown in Figure 18. The left plot shows the significant variation in center of pressure for a subject walking on hilly terrain. This variation is due to the

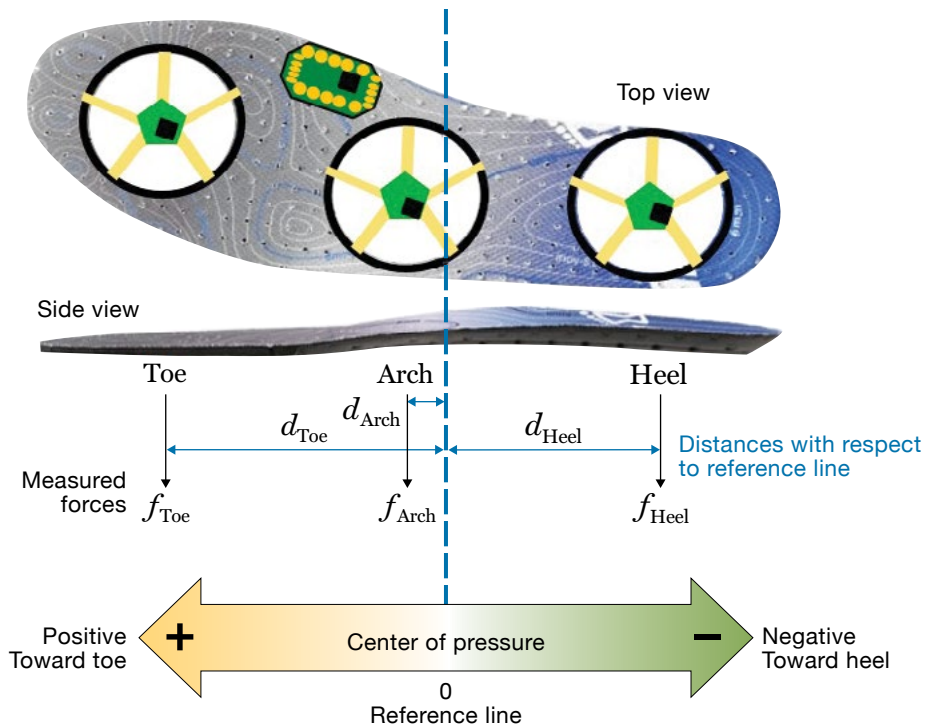


**FIGURE 17.** The center of pressure calculation for MoBILE is illustrated. When the center of pressure is negative, the user is applying more weight to the heel. When the center of pressure becomes positive, the user is applying more weight to the toes.

redistribution of weight associated with walking up and down slopes. The plot on the right compares three different instances of flat walking for the same subject. A notable shift in the center of pressure occurs as weight is added to the subject, and an additional shift happens after the subject has walked for 30 minutes with the load. While this example highlights elevation and load changes, we could also use this feature to estimate shifts in weight distribution caused by other relevant biomechanical conditions, such as a rebalancing of the load or an injury.

### Energy Expenditure

Energy expenditure is measured directly by monitoring oxygen consumption. However, this type of direct measurement can be cumbersome to collect in the field because the equipment to measure energy expenditure is bulky and not user friendly. Alternatively, a number of equations have been proposed to predict energy expenditure by using indirect measurements of parameters, such as speed, body weight, external load, and information about terrain slope and type [27]. We can use measurements from the MoBILE sensor as dynamic inputs to these predictive equations. For example, the Pandolf model with a

correction factor for negative slopes [28, 29] and the more recently developed Weyand model [30] rely only on speed, terrain slope, terrain factor, and weight. While MoBILE does not measure absolute speed, the cadence derived from the IMUs, paired with an assumed stride length (height dependent) for an individual, may be a reasonable surrogate for speed in these equations for calculating energy expenditure. Similarly, grade can be estimated from altitude rate and the assumed stride length, and total weight can be measured from intervals in the load sensor data that depict when the subject is standing.

Figure 19 shows estimates of energy expenditure (reported in volume of oxygen consumed per minute per kilogram) for the first hour of the 10-kilometer march with a load. The low energy expenditure at the beginning corresponds to a period during which the subject is standing prior to the beginning of the march. Throughout the march, the estimates of energy expenditure fluctuate, with energy expenditure increasing on the uphill stretches. In the near future, real-time calculation of energy expenditure could be possible with MoBILE or another sensor. Wearable sensors that monitor energy expenditure in real time could be important tools for determining energy intake needs and optimizing physical performance.

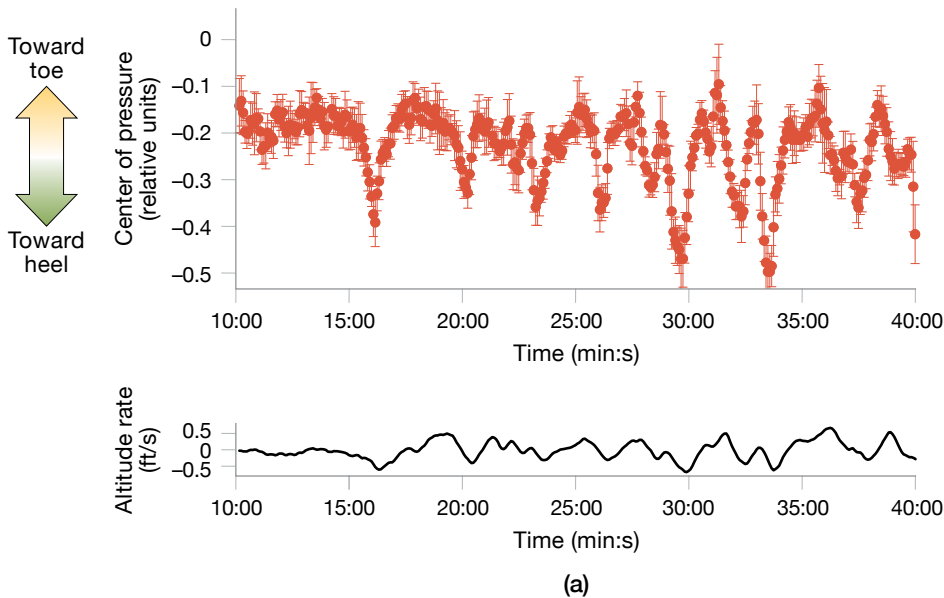
### Identifying Biomechanical Anomalies from Multimodal Measurements

Multimodal sensors, such as the ones integrated into MoBILE, are capable of measuring subtle biomechanical changes that occur in response to different physical activities. The presence of these measurable changes suggests promising potential for training machine learning algorithms to use the combined features from a rich multisensory dataset to classify the physical state of an individual.

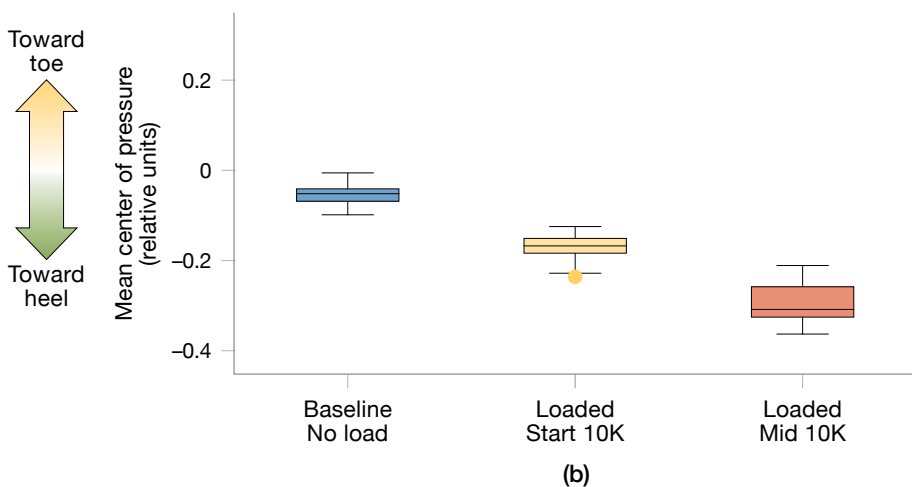
In addition to collecting data with the MoBILE sensor, we also collected heart rate, core temperature, and skin temperature measurements during the 10-kilometer march. Combining load sensors with physiological

monitoring sensors could increase the classification potential for a multimodal system. Some potential classes for machine learning might include the weight-bearing status (wearing a heavy pack versus no load), difficulty of the terrain (uphill versus downhill), index of fatigue, efficiency of load carriage, and early indications of lower-limb MSIs. While some changes in the feature values can be seen by eye, machine learning algorithms can learn to recognize subtle changes across many dimensions to provide robust estimates of the physical state.

The radar plot in Figure 20 demonstrates some of the measured differences in an eight-dimensional space that includes features derived from the load sensors, IMUs, barometers, and physiological status monitoring. The



**FIGURE 18.** The plots show the center of pressure of a subject during a data collection. The two plots in (a) compare changes in the center of pressure to changes in altitude rate. The center of pressure shifts to the toes when the altitude rate increases (uphill walking) and shifts to the heels when the altitude rate decreases (downhill walking). The plot in (b) compares the center of pressure on flat terrain during the course of a 10-kilometer march. The center of pressure changed during the march, resulting in the user carrying more of the weight on his heels. While these methods examine the effects of elevation and load carriage on weight distribution, they could also be used to detect weight distribution caused by physical conditions such as an injury.



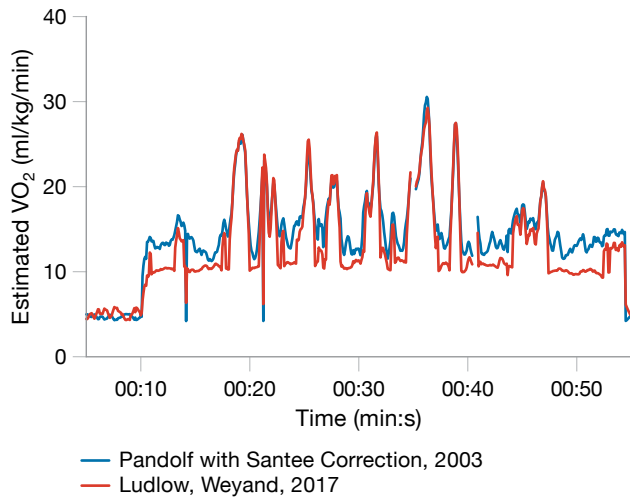


**FIGURE 19.** The chart, based on MoBILE sensor measurements, shows the dynamic estimate of energy expenditure over a 10-kilometer march on hilly terrain. Both the Pandolf and Weyand calculations match closely during periods of high exertion (high  $VO_2$ ) but differ during lower exertion. The difference is due to the fact that the Pandolf equation does not isolate the static part of the metabolic rate when the subject is just standing with the load. This characteristic of the Pandolf equation results in higher baseline metabolic rates.

three colored polygons indicate three different conditions: the baseline (no load), start of the march with a 40-pound load, and an hour into the loaded march, which we assume to correspond to a mildly fatigued state for the individual. Several features, such as the center of pressure, toe and heel force, and forward acceleration, change dramatically over the three conditions. Other features, such as medial rotation, heat strain index, and core temperature, change slightly. The significance of the amount of change for each feature has not been accounted for in this plot. For example, a slight change in core temperature can be just as significant as a large change in the center of pressure. Future work in this area includes selecting a subset of powerful features and building a classifier to predict characteristics of the individual’s physical state over time.

### Future Work

Going forward, an overarching goal is to translate data-derived features into actionable information that allows the user to assess the information and respond. For example, if a person’s gait is significantly altered to accommodate extra load, that information should be reported in an interpretable manner that highlights the

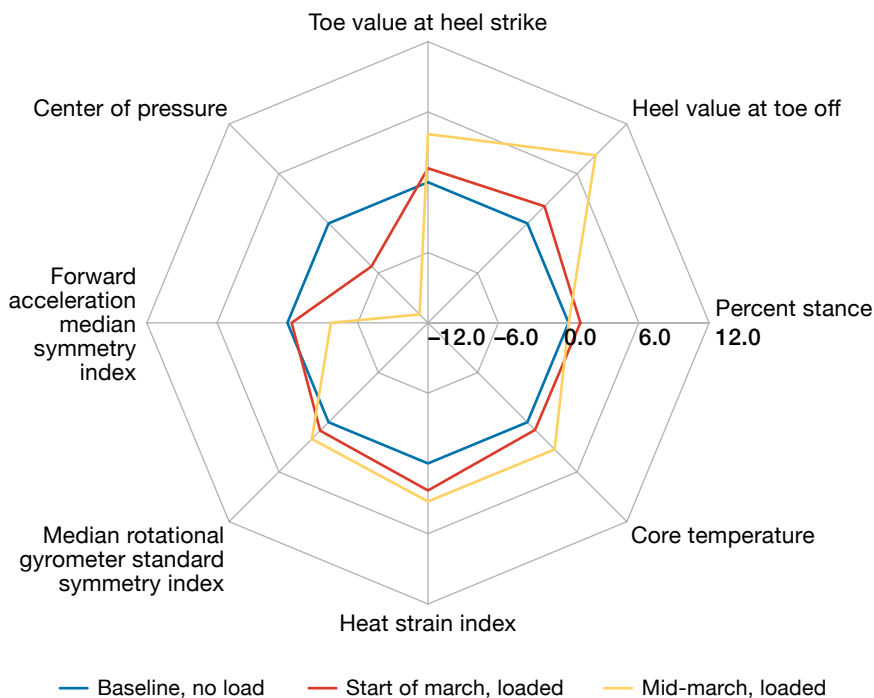


**FIGURE 20.** The radar plot depicts measured differences from eight features that are derived from the load sensors, IMUs, barometers, and physiological status monitoring. The blue, yellow, and red lines indicate feature values for the baseline (no load), mid-march, and start of march, respectively. Several of the features show little change (percent stance, heat strain index), while others change from the no-load baseline to the start of the march (loaded) and then from the start of the march to mid-march. Future work includes selecting fatigue- and injury-indicating features and building a classifier to predict characteristics of the individual’s physical state over time.

risk of injury and helps determine appropriate work-rest cycles or weight redistribution to prevent injury and optimize performance.

The ability to relate biomechanical measurements and models from within a laboratory setting to measurements in real-world environments requires capturing movement data in the field. Generating field datasets from accelerometers, instrumented inserts, or any other sensor or measurement is the first step to understanding and interpreting movement. These data need to be compared to ground truth and over a long duration. Once these data are generated, a wealth of information can be extracted from them. Current commercial systems focus on providing the user with a few snippets of information, but to be truly useful, the measurements and algorithms need to be merged. MoBILE is an attempt to provide accurate biomechanical measurement and to develop the analysis tools to extract features for the classification of movement types and potentially injured states. ■

## References

1. K.G. Hauret, B.H. Jones, S.H. Bullock, M. Canham-Chervak, and S. Canada, "Musculoskeletal Injuries Description of an Under-Recognized Injury Problem Among Military Personnel," *American Journal of Preventative Medicine*, vol. 38, no. 1, 2010, pp. S61–S70.
2. A. Yassi, "Repetitive Strain Injuries," *The Lancet*, vol. 349, no. 9066, 1997, pp. 943–947.
3. C.E. Milner, R. Ferber, C.D. Pollard, J. Hamill, and I.S. Davis, "Biomechanical Factors Associated with Tibial Stress Fracture in Female Runners," *Medicine and Science in Sports and Exercise*, vol. 38, no. 2, 2006, pp. 323–328.
4. R.B. Davis, "Clinical Gait Analysis," *IEEE Engineering in Medicine and Biology Magazine*, vol. 7, no. 3, 1988, pp. 35–40.
5. K.K. Patterson, W.H. Gage, D. Brooks, S.E. Black, and W.E. McLroy, "Evaluation of Gait Symmetry after Stroke: A Comparison of Current Methods and Recommendations for Standardization," *Gait Posture*, vol. 31, no. 2, 2010, pp. 241–246.
6. A. Salarian, H. Russmann, F.J. Vingerhoets, C. Dehollain, Y. Blanc, P.R. Burkhard, and K. Aminian, "Gait Assessment in Parkinson's Disease: Toward an Ambulatory System for Long-Term Monitoring," *IEEE Transactions on Biomedical Engineering*, vol. 51, no. 8, 2004, pp. 1434–1443.
7. C.B. Redd and S.J.M. Bamberg, "A Wireless Sensory Feedback Device for Real-Time Gait Feedback and Training," *IEEE/American Society of Mechanical Engineers (ASME) Transactions on Mechatronics*, vol. 17, no. 3, 2012, pp. 425–433.
8. K. Aminian, K. Rezakhanlou, E. De Andres, C. Fritsch, P.F. Leyvraz, and P. Robert, "Temporal Feature Estimation during Walking Using Miniature Accelerometers: An Analysis of Gait Improvement after Hip Arthroplasty," *Medical and Biological Engineering and Computing*, vol. 37, no. 6, 1999, pp. 686–691.
9. C. Hodt-Billington, J.L. Helbostad, W. Vervaat, T. Rognsvåg, and R. Moe-Milssen, "Criteria of Gait Asymmetry in Patients with Hip Osteoarthritis," *Physiotherapy Theory and Practice*, vol. 28, no. 2, 2011, pp. 134–141.
10. A. Tura, M. Raggi, L. Rocchi, A.G. Cutti, and L. Chiari, "Gait Symmetry and Regularity in Transfemoral Amputees Assessed by Trunk Accelerations," *Journal of NeuroEngineering and Rehabilitation*, vol. 7, no. 4, 2010, p. 4.
11. H. Sadeghi, P. Allard, F. Prince, and H. Labelle, "Symmetry and Limb Dominance in Able-Bodied Gait: A Review," *Gait Posture*, vol. 12, no. 1, 2000, pp. 34–45.
12. R.O. Robinson, W. Herzog, and B.M. Nigg, "Use of Force Platform Variables to Quantify the Effects of Chiropractic Manipulation on Gait Symmetry," *Journal of Manipulative and Physiological Therapeutics*, vol. 10, no. 4, 1987, pp. 172–176.
13. R. Moe-Nilssen and J.L. Helbostad, "Estimation of Gait Cycle Characteristics by Trunk Accelerometry," *Journal of Biomechanics*, vol. 37, no. 1, 2004, pp. 121–126.
14. F.A. Barber and A.N. Sutker, "Iliotibial Band Syndrome," *Sports Medicine*, vol. 14, no. 2, 1992, pp. 144–148.
15. C.M. Clements, D. Moody, A.W. Potter, J. F. Seay, R.E. Fellin, and M.J. Buller, "Loaded and Unloaded Foot Movement Differentiation Using Chest Mounted Accelerometer Signatures," paper presented at the 2013 IEEE International Conference on Body Sensor Networks, Cambridge, 6–9 May 2013.
16. J.R. Williamson, A. Dumas, G. Ciccarelli, A.R. Hess, B.A. Telfer, and M.J. Buller, "Estimating Load Carriage from a Body-Worn Accelerometer," paper in *2015 IEEE 12th International Conference on Wearable and Implantable Body Sensor Networks (BSN)*, 2015.
17. C. Liedtke, S.A. Fokkenrood, J.T. Menger, H. van der Kooij, and P.H. Veltink, "Evaluation of Instrumented Shoes for Ambulatory Assessment of Ground Reaction Forces," *Gait and Posture*, vol. 26, no. 1, 2007, pp. 39–47.
18. W. Tao, T. Liu, R. Zheng, and H. Feng, "Gait Analysis Using Wearable Sensors," *Sensors (Basel, Switzerland)*, vol. 12, no. 2, 2012, pp. 2255–2283.
19. A.H.A. Razak, A. Zayegh, R.K. Begg, and Y. Wahab, "Foot Plantar Pressure Measurement System: A Review," *Sensors (Basel, Switzerland)*, vol. 12, no. 7, 2012, pp. 9884–9912.
20. S.J. Bamberg, A.Y. Benbasat, D.M. Scarborough, D.E. Krebs, and J.A. Paradiso, "Gait Analysis Using a Shoe-Integrated Wireless Sensor System," *IEEE Transactions on Information Technology in Biomedicine*, vol. 12, no. 4, 2008, pp. 413–423.
21. A.B. Putti, G.P. Arnold, L. Cochrane, and R.J. Abboud, "The Pedar® In-Shoe System: Repeatability and Normal Pressure Values," *Gait and Posture*, vol. 35, no. 3, 2006, pp. 401–405.

22. P.H. Veltink, C. Liedtke, E. Droog, and H. van der Kooij, "Ambulatory Measurement of Ground Reaction Forces," *IEEE Transactions on Neural Systems and Rehabilitation Engineering*, vol. 13, no. 3, 2005, pp. 423–427.
23. H.M. Schepers, H.F.J.M. Koopman, and P.H. Veltink, "Ambulatory Assessment of Ankle and Foot Dynamics," *IEEE Transactions on Biomedical Engineering*, vol. 54, no. 5, 2007, pp. 895–902.
24. R.F. Lind, L.J. Love, J.C. Rowe, and F.G. Pin, "Multi-axis Foot Reaction Force/Torque Sensor for Biomedical Applications," paper in *2009 IEEE/RSJ International Conference on Intelligent Robots and Systems*, 2019.
25. J.J. Skrzypek and W.W. Ganczarski, eds., *Mechanics of Anisotropic Materials*. Switzerland: Springer International Publishing, 2015.
26. J.R. Williamson, A. Dumas, A.R. Hess, T. Patel, B.A. Telfer, and M.J. Buller, "Detecting and Tracking Gait Asymmetries with Wearable Accelerometers," paper in *2015 IEEE 12th International Conference on Wearable and Implantable Body Sensor Networks (BSN)*, 2015.
27. A.W. Potter, W.R. Santee, C.M. Clements, K.A. Brooks, and R.W. Hoyt, "Comparative Analysis of Metabolic Cost Equations: A Review," *Journal of Sport and Human Performance*, vol. 1, no. 3, 2013.
28. K.B. Pandolf, B. Givoni, and R.F. Goldman, "Predicting Energy Expenditure with Loads While Standing or Walking Very Slowly," *Journal of Applied Physiology: Respiratory, Environmental, and Exercise Physiology*, vol. 43, no. 4, 1977, pp. 577–581.
29. W.R. Santee, L.A. Blanchard, K.L. Speckman, J.A. Gonzalez, and R.F. Wallace, "Load Carriage Model Development and Testing with Field Data," U.S. Army Research Institute of Environmental Medicine Technical Note, 2003.
30. L.W. Ludlow and P.G. Weyand, "Walking Economy is Predictably Determined by Speed, Grade, and Gravitational Load," *Journal of Applied Physiology*, vol. 123, no. 5, 2017, pp. 1288–1302.

Appendix

# The Sensorimotor Technology Realization in Immersive Virtual Environments Center

**The MIT Lincoln Laboratory Sensorimotor Technology Realization in Immersive Virtual Environments (STRIVE) Center** was established in July 2016 to promote collaboration among the government, academic, and medical communities on key challenges in clinical rehabilitation, wearable technology development, and advanced operational training. The STRIVE Center’s flagship capability is the Computer-Assisted Rehabilitation Environment (CAREN), one of three such systems in the world that features a 24-foot dome. The CAREN enables the assessment of individuals’ cognitive and physiological performance as they interact with a fully immersive virtual environment. It features a 360-degree visualization screen extending from the dome onto the treadmill surface, surround sound, an 18-camera motion-capture system, a dual-belt instrumented treadmill mounted on a

six-degrees-of-freedom motion platform, and integrated sensing of electrophysiological signals and vital signs. The system is run by real-time software that allows researchers to introduce elements into the scene in a flexible manner. The facility, approximately 4,000 square feet in size, is operated by the Lincoln Laboratory Human Health and Performance Systems Group as an asset available for use by researchers throughout the Laboratory to support programs spanning all major mission areas.

**Research Focuses**

**Clinical Research**

The CAREN system offers a unique platform for clinical research by combining exceptional flexibility and precision of prescribed sensory perturbations with the simultaneous collection of multimodal physiological data. This real-time



The Sensorimotor Technology Realization in Immersive Virtual Environments (STRIVE) Center features a virtual reality dome for research and development across many mission areas.

system allows clinicians and researchers to tailor training and rehabilitation protocols to individual patients. Key focus areas within the STRIVE Center's foundational and applied clinical research programs include balance, movement, and cognitive performance.

### Technology Development

Field testing is essential to rigorously evaluate many human optimization techniques and emerging wearable technologies, such as exoskeletons, physiological status monitors, and heads-up displays. The standard laboratory setting lacks many aspects of the real world that are often not considered during the design and development of technologies. A physically and cognitively immersive environment, such as the CAREN, provides a realistic testing platform for systematic and rapid evaluation even during early design phases while capturing many gold-standard laboratory metrics. Data from such testing will provide constructive feedback to developers and enrich the technology development process.

### Operational Excellence

In challenging operational environments, field-site training is often difficult and expensive to develop, with limited opportunity for trainees to iterate through a variety of mission conditions and environments. The CAREN provides a rich and flexible serious gaming platform for operators to rapidly build experience by completing multiple scenarios in a single day. As a result, trainees, such as first responders and warfighters, can increase their physical agility, improve their mission-specific decision-making skills, and learn from their mistakes with minimal risk of injury.

### Training for Success

Developing proficiency in a specialized physical or cognitive skill often requires years of experience for a person to become a qualified expert. The multimodal sensing capabilities of the CAREN can quantify specific physical characteristics that identify individuals as experts and use them as benchmarks for training. Providing biofeedback via sensory cues assists novices to more quickly improve their skills in tasks such as dismounted marksmanship or rapid threat identification. The CAREN provides a way to learn more about the basic physiology of skilled experts and an interactive method for enhanced learning.

### About the Authors



**Joseph J. Lacirignola** is a member of the technical staff in the Counter-Weapons of Mass Destruction Systems Group. His research interests include sensor, device, and novel detection development capabilities. He joined the Laboratory in 2003 and worked on CANARY (i.e., Cellular Analysis and Notification of Antigen Risks and Yields) and related biosensing hardware platforms. Throughout his career, he has been involved in numerous hardware programs spanning biological and chemical detection, wearable sensing, novel 3D-printing hardware, multimodal detection systems, and the development of unmanned aerial and ground vehicles. He has authored several journal articles, conference presentations, and book chapters and holds more than 10 patents. He holds a bachelor's degree in biology from Syracuse University, bachelor's degrees in mechanical engineering and mechanical design from Wentworth Institute of Technology, and a master's degree in molecular and cell biology from Brandeis University.



**James R. Williamson** is a member of the technical staff in the Human Health and Performance Systems Group. His work focuses on detecting and modeling neurocognitive and physical states through the analysis of speech, facial expressions, gait, and body-sensing modalities. Prior to joining Lincoln Laboratory, he earned a bachelor's degree in psychology from the University of Massachusetts Amherst and a doctoral degree in cognitive and neural systems from Boston University. He also served as a research assistant professor at Boston University.



**Shakti K. Davis** is a member of the senior technical staff in the Human Health and Performance Systems Group. Among her research interests is the development of sensor and signal processing algorithms that are aimed at applications for protecting warfighters against injury and enhancing warfighters' performance capabilities. Since 2015, she has supported a variety of signal processing research efforts, including characterizing exposure to hazardous military noise through the use of body-worn acoustic sensors, developing algorithms to estimate risk factors of musculoskeletal injury by using foot-mounted biomechanical sensors, and investigating classification methods that use high-resolution noninvasive physiological sensors to provide early warning of virus exposure. She joined Lincoln Laboratory in 2006 and worked on detection and classification algorithms for airborne radar systems for nine years. She holds a bachelor's degree from New Mexico State University and a doctorate from the University of Wisconsin-Madison in electrical engineering.



**Whitney T. Young** was a member of the Bioengineering Systems and Technology Group for more than six years. While in the group, she contributed to a variety of projects, ranging from biodefense to synthetic biology to physiological monitoring. In her last few years at Lincoln Laboratory, she researched biome-

chanics, specifically data collection and analysis of gait in various loaded conditions, to detect and prevent musculoskeletal injuries in warfighters. She now works as a mission systems analyst at Ball Aerospace in Colorado. She holds a master's degree in mechanical engineering from MIT and a bachelor's degree in bioengineering from the University of Toledo.